

Performance Studies of Underwater Wireless Optical Communication Systems with Spatial Diversity: MIMO Scheme

Mohammad Vahid Jamali, and Jawad A. Salehi, *Fellow, IEEE*

Abstract—In this paper, we analytically study the performance of multiple-input multiple-output underwater wireless optical communication (MIMO-UWOC) systems with on-off keying (OOK) modulation. To mitigate turbulence-induced fading, which is amongst the major degrading effects of underwater channels on the propagating optical signal, we use spatial diversity over UWOC links. Furthermore, the effects of absorption and scattering are considered in our analysis. We analytically obtain the exact and the upper bound bit error rate (BER) expressions for both optimal and equal gain combining. In order to more effectively calculate the system BER, we apply Gauss-Hermite quadrature formula as well as approximation to the sum of log-normal random variables. We also apply photon-counting method to evaluate the system BER in the presence of shot noise. Our numerical results indicate an excellent match between the exact and the upper bound BER curves. Also well matches between analytical results and numerical simulations confirm the accuracy of our derived expressions. Moreover, our results show that spatial diversity can considerably improve the system performance, especially for more turbulent channels, e.g., a 3×1 MISO transmission in a 25 m coastal water link with log-amplitude variance of 0.16 can introduce 8 dB performance improvement at the BER of 10^{-9} .

Index Terms—Underwater wireless optical communications, MIMO, spatial diversity, log-normal fading channel, photon-counting approach, saddle-point approximation, optimal combining, equal gain combiner.

I. INTRODUCTION

UNDERWATER wireless optical communications (UWOC) has recently been introduced for a number of demands in various underwater applications due to its scalability, reliability and flexibility. Compared with its traditional counterpart, namely acoustic communication, optical transmission has three main advantages: higher bandwidth, better security and lower time latency. Owing to these advantages, UWOC system can be exploited in a variety of applications such as imaging, real-time video transmission, high throughput sensor networks, etc. Hence, it can be considered as an alternative to meet requirements of high speed and large data underwater communications [1], [2].

Despite all of the aforementioned advantages, UWOC is only appropriate for short range communications (typically

shorter than 100 m) with realistic average transmit powers. Studies of light in water have shown that optical beam propagation through water suffers from three major impairing phenomena, namely absorption, scattering, and turbulence [3], [4]. Various studies have been carried out to theoretically and experimentally characterize absorption and scattering effects of different water types [3], [5]. For example, mathematical modeling of an UWOC channel and its performance evaluation using radiative transfer theory have been presented in [6]. Based on experimental results in [3], [5], Tang *et al.* [1] simulated the UWOC channel by means of Monte Carlo (MC) approach with respect to the effects of absorption and scattering. They also fitted a double gamma function (DGF) to this impulse response and numerically evaluated the system BER, neglecting the turbulence effects. Furthermore, a cellular underwater wireless network based on optical code division multiple access (OCDMA) technique has recently been proposed in [7].

Unlike acoustic links, where multipath reflection induces fading on the acoustic signals, in UWOC systems optical turbulence is the major cause of fading on the propagating optical signal through turbulent seawater [8]. Optical turbulence occurs as a result of random variations of refractive index. These random variations in underwater medium mainly result from fluctuations in temperature and salinity, whereas in atmosphere they result from inhomogeneities in temperature and pressure changes [8], [9]. Although, many valuable studies have been done to characterize and mitigate turbulence-induced fading in free-space optical (FSO) communications [9]–[15], investigation of its impairing effects on the performance of UWOC systems has received relatively less attention. However, recently some useful results have been reported in literature to characterize underwater fading statistics. A precise power spectrum has been derived in [4] for fluctuations of turbulent seawater refractive index. Based on this power spectrum, statistical properties of Gaussian beam propagating through turbulent water have been studied by Korotkova *et al.* [16], [17]. Also Tang *et al.* [8] have shown that temporal correlation of irradiance may be introduced by moving medium and they investigated temporal statistics of irradiance in moving ocean with weak turbulence. Moreover, Rytov method has been applied in [16], [18] to evaluate the scintillation index of optical plane and spherical waves propagating in underwater turbulent medium. Furthermore in [19], the on-axis scintillation index of a focused Gaussian beam has been formulated in weak oceanic turbulence and by

The authors are with the Optical Networks Research Laboratory (ONRL), Department of Electrical Engineering, Sharif University of Technology, Tehran, Iran (e-mail: mohammad.v.jamali@gmail.com; j.salehi@sharif.edu). This paper was presented in part at the IEEE International Workshop on Wireless Optical Communication (IWOW), Istanbul, Turkey, September 2015.

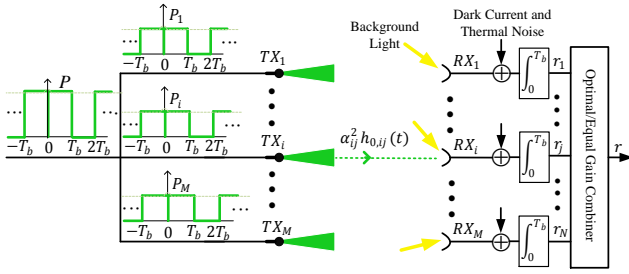


Fig. 1. Block diagram of the MIMO-UWOC system with OOK modulation.

considering log-normal distribution for intensity fluctuations, the average BER is evaluated.

In spite of all valuable presented works in various aspects of UWOC, a comprehensive study on the performance of UWOC systems that takes all degrading effects of the channel into account, is missing in the literature. The research in this paper is inspired by the need to comprehensively evaluate the BER of UWOC systems with respect to all impairing effects of the channel and also to design an UWOC system supporting longer range communications with realistic transmit powers. Spatial diversity technique, i.e., exploiting multiple transmitter/receiver apertures (see Fig. 1), not only compensates for fading effects, but can also effectively decrease the possibility of temporary blockage of the optical beam by obstruction (e.g., fishes). Another advantage of spatial diversity is in reducing the transmit power density by dividing the total transmitted power by the number of transmitters. In other words, depending on the used wavelength there exist some limitations on the maximum allowable safe transmit power. Hence, by employing spatial diversity one can increase the total transmitted power by the number of transmitters and therefore support longer distances, while maintaining the safe transmit power density [9]. In this paper, we analytically obtain the BER expressions for MIMO-UWOC systems, when either optimal combiner (OC) or equal gain combiner (EGC) is used. We also apply photon-counting approach to evaluate the BER of various configurations. In order to take into account the absorption and scattering effects, we obtain the channel impulse response by MC simulations similar to [1], [20]. To characterize fading effect, we multiply the above impulse response by a fading coefficient modeled as a log-normal random variable (RV) for weak oceanic turbulence [19], [21]. In addition to the exact BER calculation, we also evaluate the upper bound on the system BER. In our numerical results we consider both spatially independent and spatially correlated links.

The rest of the paper is organized as follows. In Section II, we review some necessary theories in the context of our proposed MIMO-UWOC system and the channel under consideration in this paper. In Section III, we analytically obtain both the exact and the upper bound BER expressions, when either OC or EGC is used at the receiver side. We also apply Gauss-Hermite quadrature formula to effectively

calculate multi-dimensional integrals with multi-dimensional finite series. In order to evaluate the system BER using photon-counting methods, the same steps as Section III are followed in Section IV. Section V presents the numerical results for various system configurations and parameters considering log-normal distribution for fading statistics of the UWOC channel, and Section VI concludes.

II. CHANNEL AND SYSTEM MODEL

In this section, we present the channel model which includes all three impairing effects of the medium, followed by the assumptions and system model that we have introduced in this paper.

A. Absorption and Scattering of UWOC Channels

Propagation of optical beam in underwater medium induces interactions between each photon and seawater particles either in the form of absorption or scattering. Absorption is an irremediable process where photons interact with water molecules and other particles and lose their energy thermally. On the other hand, in the scattering process each photon's transmit direction alters, which also can cause energy loss since less photons will be captured by the receiver aperture. Energy loss of non-scattered light due to absorption and scattering can be characterized by absorption coefficient $a(\lambda)$ and scattering coefficient $b(\lambda)$, respectively, where λ denotes the wavelength of the propagating light wave. Moreover, total effects of absorption and scattering on the energy loss can be described by extinction coefficient $c(\lambda) = a(\lambda) + b(\lambda)$. These coefficients can vary with source wavelength λ and water types [1]. It has been shown in [3], [22] that absorption and scattering have lowest effects at the wavelength interval of $400 \text{ nm} < \lambda < 530 \text{ nm}$. Hence, UWOC systems apply the blue/green region of the visible light spectrum to actualize data communication.

In [1], [20] the channel impulse response has been simulated based on MC method with respect to the absorption and scattering effects. We also simulate the channel impulse response similar to [1], [20] relying on MC approach. In this paper, the fading-free impulse response between the i th transmitter and the j th receiver is denoted by $h_{0,ij}(t)$. As it is elaborated in [1], when the source beam divergence angle and the link distance increase the channel introduces more inter-symbol interference (ISI) and loss on the received optical signal. On the other hand, increasing the receiver field of view (FOV) and aperture size increases the channel delay spread but decreases its loss.

B. Fading Statistics of UWOC Channels

In the previous subsection we described how the absorption and scattering effects are characterized. To take turbulence effects into account, we multiply $h_{0,ij}(t)$ by a multiplicative fading coefficient α_{ij}^2 [9]–[14], with log-normal distribution for weak oceanic turbulence [19], [21]. To model turbulence-induced fading let $\alpha = \exp(X)$ be the fading amplitude of the

channel with log-normal probability density function (PDF) as [23];

$$f_\alpha(\alpha) = \frac{1}{\alpha\sqrt{2\pi\sigma_X^2}} \exp\left(-\frac{(\ln(\alpha) - \mu_X)^2}{2\sigma_X^2}\right). \quad (1)$$

Therefore, the fading log-amplitude X has a Gaussian distribution with mean μ_X and variance σ_X^2 . To ensure that fading neither amplifies nor attenuates the average power, we normalize fading amplitude such that $\mathbb{E}[\alpha^2] = 1$, which implies $\mu_X = -\sigma_X^2$ [23]. In order to thoroughly describe fading statistics of UWOC channels we should find out the dependency of log-amplitude variance to the ocean turbulence parameters.

The scintillation index of a light wave is defined by [10], [16];

$$\sigma_I^2(r, d_0, \lambda) = \frac{\langle I^2(r, d_0, \lambda) \rangle - \langle I(r, d_0, \lambda) \rangle^2}{\langle I(r, d_0, \lambda) \rangle^2}, \quad (2)$$

in which $I(r, d_0, \lambda)$ is the instantaneous intensity at a point with position vector $(r, d_0) = (x, y, d_0)$, where d_0 is the propagation distance and $\langle \cdot \rangle$ denotes the long-time average. Assuming weak turbulence, the scintillation index of plane and spherical waves can be obtained as [10], [16];

$$\sigma_I^2 = 8\pi^2 k_0^2 d_0 \int_0^1 \int_0^\infty \kappa \Phi_n(\kappa) \times \left\{ 1 - \cos \left[\frac{d_0 \kappa^2}{k_0} \xi (1 - (1 - \Theta)\xi) \right] \right\} d\kappa d\xi, \quad (3)$$

in which $\Theta = 1$ and 0 for plane and spherical waves, respectively. $k_0 = 2\pi/\lambda$ and κ denote the wave number and scalar spatial frequency, respectively; and $\Phi_n(\kappa)$ is the power spectrum of turbulent fluctuations which has the form [4], [16];

$$\Phi_n(\kappa) = 0.388 \times 10^{-8} \varepsilon^{-1/3} \kappa^{-11/3} \left[1 + 2.35(\kappa\zeta)^{2/3} \right] \times \frac{\chi_T}{w^2} (w^2 e^{-A_T \delta} + e^{-A_S \delta} - 2w e^{-A_{TS} \delta}), \quad (4)$$

where ε is the rate of dissipation of turbulent kinetic energy per unit mass of fluid which can vary in the range of $10^{-2} \text{ m}^2/\text{s}^3$ to $10^{-8} \text{ m}^2/\text{s}^3$ [24], $\zeta = 10^{-3} \text{ m}$ is the Kolmogorov micro-scale, χ_T is the rate of dissipation of mean-square temperature that can take on values between $10^{-4} \text{ K}^2/\text{s}$ and $10^{-10} \text{ K}^2/\text{s}$ [24], and w (unitless) denotes the relative strength of temperature and salinity fluctuations which in ocean waters takes on values in the interval $[-5, 0]$. When dominant fluctuations are due to temperature or salinity, w takes the values close to -5 or 0 , respectively [4], [8]. Other parameters are as $A_T = 1.863 \times 10^{-2}$, $A_S = 1.9 \times 10^{-4}$, $A_{TS} = 9.41 \times 10^{-3}$ and $\delta = 8.284(\kappa\zeta)^{4/3} + 12.978(\kappa\zeta)^2$ [16]. For log-normal turbulent channels the scintillation index relates to the log-amplitude variance as $\sigma_I^2 = \exp(4\sigma_X^2) - 1$ [10]. In [16], [18] the scintillation index of plane and spherical waves has been evaluated numerically versus communication distance d_0 for various values of w , χ_T and ε . From these references it has been concluded that as w and χ_T increase the scintillation index also increases; however for larger values of ε smaller values of scintillation index are expected. Depending on these parameters, strong turbulence (which corresponds to

$\sigma_I^2 \geq 1$ [10], [16]) can occur at distances as long as 100 m and as short as 10 m, which impressively differs from atmospheric channels where strong turbulence distances are on the order of kilometers [16]. Therefore, mitigating such a strong turbulence demands more attention.

C. MIMO-UWOC System Model

We consider an UWOC system where the information signal is transmitted by M transmitters, received by N apertures and combined using OC/EGC. As it is depicted in Fig. 1, optical signal through propagation from the i th transmitter TX_i to the j th receiver RX_j experiences absorption, scattering and turbulence, where in this paper absorption and scattering are modeled by fading-free impulse response of $h_{0,ij}(t)$ (as discussed in Section II-A) and turbulence is characterized by a multiplicative fading coefficient α_{ij}^2 , which has a log-normal distribution for weak oceanic turbulence (as investigated in Section II-B). Therefore, the TX_i to RX_j channel has the aggregated impulse response of $h_{i,j}(t) = \alpha_{ij}^2 h_{0,ij}(t)$.

We assume OOK signaling where the “ON” state signal will be transmitted with the pulse shape $P(t)$. In the special case of rectangular pulse, $P(t)$ can be represented as $P(t) = P\Pi\left(\frac{t-T_b/2}{T_b}\right)$, where T_b is the bit duration time and $\Pi(t)$ is a rectangular pulse with unit amplitude in the interval $[-1/2, 1/2]$. Therefore, the transmitted signal can be expressed as;

$$S(t) = \sum_{k=-\infty}^{\infty} b_k P(t - kT_b), \quad (5)$$

where $b_k \in \{0, 1\}$ is the k th time slot transmitted bit. Hence, the received optical signal after propagating through the channel can be represented as;

$$y(t) = S(t) * \alpha^2 h_0(t) = \sum_{k=-\infty}^{\infty} b_k \alpha^2 \Gamma(t - kT_b), \quad (6)$$

in which $h_0(t)$ is the channel fading-free impulse response and $\Gamma(t) = h_0(t) * P(t)$, where $*$ denotes the convolution operator.

When M transmitters are used, in order to have a fair comparison with the single transmitter case, we assume that the total transmitted power for “ON” state signal is yet $P = \sum_{i=1}^M P_i$, where P_i is the transmitted power by TX_i . In this regard, we denote the transmitted pulse from TX_i by $P_i(t) = P_i \Pi\left(\frac{t-T_b/2}{T_b}\right)$ and also a sequence of data signal from TX_i is denoted by $S_i(t) = \sum_{k=-\infty}^{\infty} b_k P_i(t - kT_b)$. This signal reaches RX_j after propagation through the channel with impulse response of $\alpha_{ij}^2 h_{0,ij}(t)$. Hence, the transferred optical signal from TX_i to RX_j will be as follows;

$$y_{i,j}(t) = S_i(t) * \alpha_{ij}^2 h_{0,ij}(t) = \sum_{k=-\infty}^{\infty} b_k \alpha_{ij}^2 \Gamma_{i,j}(t - kT_b), \quad (7)$$

where $\Gamma_{i,j}(t) = P_i(t) * h_{0,ij}(t)$. At the j th receiver, transmitted signals from all transmitters are captured, each with its own channel impulse response. In other words, received optical signal at the j th receiver is as $y_j(t) = \sum_{i=1}^M y_{i,j}(t)$

[9], [12]. Moreover, in order to have a fair comparison between multiple receivers and single receiver cases, we assume that sum of all receiving apertures in multiple receivers scheme is equal to the receiver aperture size of single receiver scheme. We should emphasize that all of the expressions in the rest of this paper are based on $\Gamma_{i,j}(t)$, which is in terms of $P_i(t)$ and $h_{0,ij}(t)$. Therefore, our analytical expressions are applicable for any form of power allocation between different transmit apertures, any pulse shape of transmitted signal $P_i(t)$, and any channel model. However, our numerical results are based on equal power allocation for transmitters, i.e., $P_i = P/M$, $i = 1, \dots, M$, rectangular pulse for OOK signaling, MC-based simulated channel impulse response and log-normal distribution for fading statistics.

III. BER ANALYSIS

In this section, we analytically derive the exact and the upper bound BER expressions for both single-input single-output (SISO) and MIMO schemes, when either OC or EGC is used. Various noise components, i.e., background light, dark current, thermal noise and signal-dependent shot noise all affect the system performance. Since these components are additive and independent of each other, in this section we model them as an equivalent noise component with Gaussian distribution [25]. Also as it is shown in [26], the signal-dependent shot noise has a negligible effect with respect to the other noise components. Hence, it is amongst the other assumptions of this section to consider the noise variance independent to the incoming signal power. Moreover, we assume symbol-by-symbol processing at the receiver side, which is suboptimal in the presence of ISI [27]. In other words, the receiver integrates its output current over each T_b seconds and then compares the result with an appropriate threshold to detect the received data bit. In this detection process, the availability of channel state information (CSI) is also assumed for threshold calculation.

A. SISO-UWOC Link

In SISO scheme, the photodetector's 0th time slot integrated current can be expressed as¹:

$$r_{\text{SISO}}^{(b_0)} = b_0 \alpha^2 \gamma^{(s)} + \alpha^2 \sum_{k=-L}^{-1} b_k \gamma^{(I,k)} + v_{T_b}, \quad (8)$$

where $\gamma^{(s)} = R \int_0^{T_b} \Gamma(t) dt$, $\gamma^{(I,k)} = R \int_0^{T_b} \Gamma(t - kT_b) dt = R \int_{-kT_b}^{-(k-1)T_b} \Gamma(t) dt$, $R = \eta q / hf$ is the photodetector's responsivity, η is the photodetector's quantum efficiency, $q = 1.602 \times 10^{-19}$ C is electron charge, $h = 6.626 \times 10^{-34}$ J/s is Planck's constant, f is the optical source frequency and L is the channel memory. Physically, $\gamma^{(I,k \neq 0)}$ refers to the ISI effect and $\gamma^{(I,k=0)}$ interprets the desired signal contribution, i.e., $\gamma^{(I,k=0)} = \gamma^{(s)}$. Furthermore, v_{T_b} is the receiver integrated noise component, which has a Gaussian distribution with mean zero and variance $\sigma_{T_b}^2$ [25].

¹Based on the numerical results presented in [8], the channel correlation time is on the order of 10^{-5} to 10^{-2} seconds which implies that thousands up to millions of consecutive bits have the same fading coefficient. Therefore, we have adopted the same fading coefficient for all consecutive bits in Eq. (8).

Assuming the availability of CSI, the receiver compares its integrated current over each T_b seconds with an appropriate threshold, i.e., with $\tilde{T} = \alpha^2 \gamma^{(s)} / 2$. Therefore, the conditional probabilities of error when bits "1" and "0" are transmitted can respectively be obtained as;

$$P_{be|1,\alpha,b_k}^{(\text{SISO})} = \Pr(r_{\text{SISO}}^{(b_0)} \leq \tilde{T} | b_0 = 1) = Q \left(\frac{\alpha^2 [\gamma^{(s)} / 2 + \sum_{k=-L}^{-1} b_k \gamma^{(I,k)}]}{\sigma_{T_b}} \right), \quad (9)$$

$$P_{be|0,\alpha,b_k}^{(\text{SISO})} = \Pr(r_{\text{SISO}}^{(b_0)} \geq \tilde{T} | b_0 = 0) = Q \left(\frac{\alpha^2 [\gamma^{(s)} / 2 - \sum_{k=-L}^{-1} b_k \gamma^{(I,k)}]}{\sigma_{T_b}} \right), \quad (10)$$

where $Q(x) = (1/\sqrt{2\pi}) \int_x^\infty \exp(-y^2/2) dy$ is the Gaussian-Q function. The final BER can be obtained by averaging the conditional BER $P_{be|\alpha,b_k}^{(\text{SISO})} = \frac{1}{2} P_{be|0,\alpha,b_k}^{(\text{SISO})} + \frac{1}{2} P_{be|1,\alpha,b_k}^{(\text{SISO})}$ over fading coefficient α and all 2^L possible data sequences for b_k s, i.e.,

$$P_{be}^{(\text{SISO})} = \frac{1}{2^L} \sum_{b_k} \int_0^\infty P_{be|\alpha,b_k}^{(\text{SISO})} f_\alpha(\alpha) d\alpha. \quad (11)$$

The forms of Eqs. (9) and (10) suggest an upper bound on the system BER, from the ISI point of view. In other words, $b_{k \neq 0} = 0$ maximizes (9), while (10) has its maximum value for $b_{k \neq 0} = 1$. Indeed, when data bit "0" is sent the worst effect of ISI occurs when all the surrounding bits are "1" (i.e., when $b_{k \neq 0} = 1$), and vice versa [27]. Regarding these special sequences, the upper bound on the BER of SISO-UWOC system can be evaluated as;

$$P_{be,\text{UB}}^{(\text{SISO})} = \frac{1}{2} \int_0^\infty \left[Q \left(\frac{\alpha^2 \gamma^{(s)}}{2\sigma_{T_b}} \right) + Q \left(\frac{\alpha^2 [\gamma^{(s)} / 2 - \sum_{k=-L}^{-1} \gamma^{(I,k)}]}{\sigma_{T_b}} \right) \right] f_\alpha(\alpha) d\alpha. \quad (12)$$

The averaging over fading coefficient in (11) and (12) involves integrals of the form $\int_0^\infty Q(C\alpha^2) f_\alpha(\alpha) d\alpha$, where C is a constant, e.g., $C = \gamma^{(s)} / 2\sigma_{T_b}$ in the first integral of (12). Such integrals can be effectively calculated using Gauss-Hermite quadrature formula [28, Eq. (25.4.46)] as follows;

$$\begin{aligned} & \int_0^\infty Q(C\alpha^2) f_\alpha(\alpha) d\alpha \\ &= \int_{-\infty}^\infty Q(Ce^{2x}) \frac{1}{\sqrt{2\pi\sigma_X^2}} \exp \left(-\frac{(x - \mu_X)^2}{2\sigma_X^2} \right) dx \\ &\approx \frac{1}{\sqrt{\pi}} \sum_{q=1}^U w_q Q \left(C \exp \left(2x_q \sqrt{2\sigma_X^2} + 2\mu_X \right) \right), \end{aligned} \quad (13)$$

in which U is the order of approximation, w_q , $q = 1, 2, \dots, U$, are weights of the U th-order approximation and x_q is the q th zero of the U th-order Hermite polynomial, $H_U(x)$ [9], [28].

B. MIMO-UWOC Link with OC

Relying on (7), the integrated current of the j th receiver can be expressed as;

$$r_j^{(b_0)} = b_0 \sum_{i=1}^M \alpha_{ij}^2 \gamma_{i,j}^{(s)} + \sum_{i=1}^M \alpha_{ij}^2 \sum_{k=-L_{ij}}^{-1} b_k \gamma_{i,j}^{(I,k)} + v_{T_b}^{(j)}, \quad (14)$$

where $\gamma_{i,j}^{(s)} = R \int_0^{T_b} \Gamma_{i,j}(t) dt$, $\gamma_{i,j}^{(I,k)} = R \int_0^{T_b} \Gamma_{i,j}(t - kT_b) dt = R \int_{-kT_b}^{-(k-1)T_b} \Gamma_{i,j}(t) dt$, $L_{i,j}$ is the memory of the channel between the i th transmitter and the j th receiver, and $v_{T_b}^{(j)}$ is the j th receiver integrated noise, which has a Gaussian distribution with mean zero and variance $\sigma_{T_b}^2$. Assuming the availability of perfect CSI, the symbol-by-symbol receiver which does not have any knowledge to $\{b_k\}_{k=-L_{i,j}}^{-1}$, adopts the following metric for optimum combining [9];

$$\Pr(\vec{r}|b_0 = 1, \vec{\alpha}) \stackrel{1}{\geq} \Pr(\vec{r}|b_0 = 0, \vec{\alpha}), \quad (15)$$

where $\vec{r} = (r_1, r_2, \dots, r_N)$ is the vector of different branches' integrated received current and $\vec{\alpha} = (\alpha_{11}, \alpha_{12}, \dots, \alpha_{MN})$ is the fading coefficients vector. The conditional probabilities for "ON" and "OFF" states are respectively given as;

$$\Pr(\vec{r}|b_0 = 1, \vec{\alpha}) = \frac{1}{(2\pi\sigma_{T_b}^2)^{N/2}} \exp\left(\frac{-1}{2\sigma_{T_b}^2} \sum_{j=1}^N \left[r_j - \sum_{i=1}^M \alpha_{ij}^2 \gamma_{i,j}^{(s)}\right]^2\right), \quad (16)$$

$$\Pr(\vec{r}|b_0 = 0, \vec{\alpha}) = \frac{1}{(2\pi\sigma_{T_b}^2)^{N/2}} \exp\left(\frac{-1}{2\sigma_{T_b}^2} \sum_{j=1}^N r_j^2\right). \quad (17)$$

Replacing (16) and (17) in (15) and dropping the common terms out, the decision rule simplifies to;

$$\sum_{j=1}^N 2r_j \sum_{i=1}^M \alpha_{ij}^2 \gamma_{i,j}^{(s)} \stackrel{1}{\geq} \sum_{j=1}^N \left(\sum_{i=1}^M \alpha_{ij}^2 \gamma_{i,j}^{(s)}\right)^2. \quad (18)$$

Using the above decision rule, we can find the "ON" and "OFF" states conditional error probabilities as Eqs. (19) and (20), respectively, shown at the top of the next page. Assuming the maximum channel memory as $L_{\max} = \max\{L_{11}, L_{12}, \dots, L_{MN}\}$, the average BER of MIMO-UWOC system can be obtained by averaging over $\vec{\alpha}$ (through an $(M \times N)$ -dimensional integral) as well as averaging over all $2^{L_{\max}}$ possible sequences for b_k s, i.e.,

$$P_{be}^{(MIMO)} = \frac{1}{2^{L_{\max}}} \sum_{b_k} \int_{\vec{\alpha}} \frac{1}{2} \left[P_{be|1, \vec{\alpha}, b_k}^{(MIMO)} + P_{be|0, \vec{\alpha}, b_k}^{(MIMO)} \right] f_{\vec{\alpha}}(\vec{\alpha}) d\vec{\alpha}, \quad (21)$$

where $f_{\vec{\alpha}}(\vec{\alpha})$ is the joint PDF of fading coefficients in $\vec{\alpha}$.

Furthermore, considering the transmitted data sequences as $b_{k \neq 0} = 1$ for $b_0 = 0$ and $b_{k \neq 0} = 0$ for $b_0 = 1$, the upper bound on the BER of MIMO-UWOC system can be obtained as Eq. (22), shown at the top of the next page. Moreover, as it is shown in Appendix A, $(M \times N)$ -dimensional integrals

in (21) and (22) can effectively be calculated by $(M \times N)$ -dimensional series using Gauss-Hermite quadrature formula.

It is worth mentioning that for transmitter diversity ($N = 1$) the conditional BER expressions in (19) and (20) simplify to the following equation;

$$P_{be|b_0, \vec{\alpha}, b_k}^{(MISO)} = Q\left(\sum_{i=1}^M \alpha_{i1}^2 \left[\gamma_{i,1}^{(s)} + (-1)^{b_0+1} \sum_{k=-L_{i1}}^{-1} 2b_k \gamma_{i,1}^{(I,k)}\right] / 2\sigma_{T_b}\right), \quad (23)$$

which can be reformulated as $P_{be|b_0, \vec{\alpha}, b_k}^{(MISO)} = Q\left(\sum_{i=1}^M \alpha_{i1}^2 G_{i,1}^{(b_0)}\right)$, where $G_{i,1}^{(b_0)} = [\gamma_{i,1}^{(s)} + (-1)^{b_0+1} \sum_{k=-L_{i1}}^{-1} 2b_k \gamma_{i,1}^{(I,k)}] / 2\sigma_{T_b}$. The weighted sum of RVs in (23) can be approximated by an equivalent RV, using moment matching method [29]. Therefore, we can approximate the conditional BER of (23) as $P_{be|b_0, \vec{\alpha}, b_k}^{(MISO)} \approx Q\left(G_M^{(b_0)}\right)$, where $G_M^{(b_0)}$ is the equivalent RV resulted from approximation to the weighted sum of RVs, i.e., $G_M^{(b_0)} \approx \sum_{i=1}^M \alpha_{i1}^2 G_{i,1}^{(b_0)}$. In the special case of log-normal fading the equivalent log-normal RV, $G_M^{(b_0)} = \exp(2z^{(b_0)})$, has log-amplitude mean and variance of;

$$\mu_{z^{(b_0)}} = \frac{1}{2} \ln\left(\sum_{i=1}^M G_{i,1}^{(b_0)}\right) - \sigma_{z^{(b_0)}}^2, \quad (24)$$

$$\sigma_{z^{(b_0)}}^2 = \frac{1}{4} \ln\left(1 + \frac{\sum_{i=1}^M \left(G_{i,1}^{(b_0)}\right)^2 \left(e^{4\sigma_{x_{i1}}^2} - 1\right)}{\left(\sum_{i=1}^M G_{i,1}^{(b_0)}\right)^2}\right), \quad (25)$$

respectively [23]. Hence, in the case of transmitter diversity the average BER can be approximately evaluated with a one-dimensional integral which can also be calculated using Gauss-Hermite quadrature formula as a one-dimensional series.

C. MIMO-UWOC Link with EGC

When EGC is used, the integrated current of the receiver output can be expressed as;

$$r_{\text{MIMO}}^{(b_0)} = b_0 \sum_{j=1}^N \sum_{i=1}^M \alpha_{ij}^2 \gamma_{i,j}^{(s)} + \sum_{j=1}^N \sum_{i=1}^M \alpha_{ij}^2 \sum_{k=-L_{ij}}^{-1} b_k \gamma_{i,j}^{(I,k)} + v_{T_b}^{(N)}, \quad (26)$$

where $v_{T_b}^{(N)}$ is the integrated combined noise component which has a Gaussian distribution with mean zero and variance $N\sigma_{T_b}^2$ [26].

Based on (26) and the availability of CSI, the receiver selects the threshold value as $\tilde{T} = \sum_{j=1}^N \sum_{i=1}^M \alpha_{ij}^2 \gamma_{i,j}^{(s)} / 2$. Pursuing similar steps as Section III-B results to (27) for conditional BER. As expected, (27) simplifies to (23) for multiple-input single-output (MISO) scheme. Finally, the average BER can be evaluated similar to (21). Also the upper bound on the BER of MIMO-UWOC system with EGC can be expressed as Eq. (28), shown at the top of the next page.

It is worth noting that the numerator of (27) can be approximated as $\zeta^{(b_0)} \approx \sum_{j=1}^N \sum_{i=1}^M D_{i,j}^{(b_0)} \alpha_{ij}^2$, where

$$\begin{aligned}
P_{be|1,\vec{\alpha},b_k}^{(\text{MIMO})} &= \Pr \left(\sum_{j=1}^N 2r_j \sum_{i=1}^M \alpha_{ij}^2 \gamma_{i,j}^{(s)} \leq \sum_{j=1}^N \left(\sum_{i=1}^M \alpha_{ij}^2 \gamma_{i,j}^{(s)} \right)^2 \mid r_j = \sum_{i=1}^M \alpha_{ij}^2 \gamma_{i,j}^{(s)} + \sum_{i=1}^M \alpha_{ij}^2 \sum_{k=-L_{ij}}^{-1} b_k \gamma_{i,j}^{(I,k)} + v_{T_b}^{(j)}, \vec{\alpha}, b_k \right) \\
&= \Pr \left(\sum_{j=1}^N \left[2v_{T_b}^{(j)} \sum_{i=1}^M \alpha_{ij}^2 \gamma_{i,j}^{(s)} \right] \leq - \sum_{j=1}^N \sum_{i'=1}^M \alpha_{i'j}^2 \gamma_{i',j}^{(s)} \sum_{i=1}^M \alpha_{ij}^2 \left(\gamma_{i,j}^{(s)} + 2 \sum_{k=-L_{ij}}^{-1} b_k \gamma_{i,j}^{(I,k)} \right) \right) \\
&= Q \left(\frac{\sum_{j=1}^N \sum_{i'=1}^M \alpha_{i'j}^2 \gamma_{i',j}^{(s)} \sum_{i=1}^M \alpha_{ij}^2 \left(\gamma_{i,j}^{(s)} + 2 \sum_{k=-L_{ij}}^{-1} b_k \gamma_{i,j}^{(I,k)} \right)}{2\sigma_{T_b} \sqrt{\sum_{j=1}^N \left(\sum_{i=1}^M \alpha_{ij}^2 \gamma_{i,j}^{(s)} \right)^2}} \right). \tag{19}
\end{aligned}$$

$$P_{be|0,\vec{\alpha},b_k}^{(\text{MIMO})} = Q \left(\frac{\sum_{j=1}^N \sum_{i'=1}^M \alpha_{i'j}^2 \gamma_{i',j}^{(s)} \sum_{i=1}^M \alpha_{ij}^2 \left(\gamma_{i,j}^{(s)} - 2 \sum_{k=-L_{ij}}^{-1} b_k \gamma_{i,j}^{(I,k)} \right)}{2\sigma_{T_b} \sqrt{\sum_{j=1}^N \left(\sum_{i=1}^M \alpha_{ij}^2 \gamma_{i,j}^{(s)} \right)^2}} \right). \tag{20}$$

$$P_{be,\text{UB}}^{(\text{MIMO})} = \int_{\vec{\alpha}} \frac{1}{2} \left[Q \left(\frac{\sqrt{\sum_{j=1}^N \left(\sum_{i=1}^M \alpha_{ij}^2 \gamma_{i,j}^{(s)} \right)^2}}{2\sigma_{T_b}} \right) + Q \left(\frac{\sum_{j=1}^N \sum_{i'=1}^M \alpha_{i'j}^2 \gamma_{i',j}^{(s)} \sum_{i=1}^M \alpha_{ij}^2 \left(\gamma_{i,j}^{(s)} - 2 \sum_{k=-L_{ij}}^{-1} b_k \gamma_{i,j}^{(I,k)} \right)}{2\sigma_{T_b} \sqrt{\sum_{j=1}^N \left(\sum_{i=1}^M \alpha_{ij}^2 \gamma_{i,j}^{(s)} \right)^2}} \right) \right] f_{\vec{\alpha}}(\vec{\alpha}) d\vec{\alpha}. \tag{22}$$

$$P_{be|b_0,\vec{\alpha},b_k}^{(\text{MIMO})} = Q \left(\frac{\sum_{j=1}^N \sum_{i=1}^M \alpha_{ij}^2 \gamma_{i,j}^{(s)} + (-1)^{b_0+1} \sum_{j=1}^N \sum_{i=1}^M \alpha_{ij}^2 \sum_{k=-L_{ij}}^{-1} 2b_k \gamma_{i,j}^{(I,k)}}{2\sqrt{N}\sigma_{T_b}} \right). \tag{27}$$

$$P_{be,\text{UB}}^{(\text{MIMO})} = \int_{\vec{\alpha}} \frac{1}{2} \left[Q \left(\frac{\sum_{j=1}^N \sum_{i=1}^M \alpha_{ij}^2 \gamma_{i,j}^{(s)}}{2\sqrt{N}\sigma_{T_b}} \right) + Q \left(\frac{\sum_{j=1}^N \sum_{i=1}^M \alpha_{ij}^2 \left[\gamma_{i,j}^{(s)} - 2 \sum_{k=-L_{ij}}^{-1} b_k \gamma_{i,j}^{(I,k)} \right]}{2\sqrt{N}\sigma_{T_b}} \right) \right] f_{\vec{\alpha}}(\vec{\alpha}) d\vec{\alpha}. \tag{28}$$

the weight coefficients are defined as $D_{i,j}^{(b_0)} = \gamma_{i,j}^{(s)} + (-1)^{b_0+1} \sum_{k=-L_{ij}}^{-1} 2b_k \gamma_{i,j}^{(I,k)}$. Similar to (24) and (25), statistics of the equivalent log-normal RV $\zeta^{(b_0)}$, which is resulted from weighted sum of $M \times N$ RVs, can be obtained and then averaging over fading coefficients reduces to one-dimensional integral of;

$$P_{be|b_0,b_k}^{(\text{MIMO})} \approx \int_0^\infty Q \left(\frac{\zeta^{(b_0)}}{2\sqrt{N}\sigma_{T_b}} \right) f_{\zeta^{(b_0)}}(\zeta^{(b_0)}) d\zeta^{(b_0)}, \tag{29}$$

which can also effectively be calculated using Eq. (13).

IV. BER EVALUATION USING PHOTON-COUNTING METHODS

In this section, we derive the required expressions for the system BER using photon-counting approach. Moreover, in this section signal-dependent shot noise, dark current and background light all are considered with Poisson distribution, while thermal noise is assumed to be Gaussian distributed [27]. To evaluate the BER, we can apply either saddle-point approximation or Gaussian approximation which is simpler but negligibly less accurate than saddle-point approximation.

Based on saddle-point approximation the system BER can be obtained as $P_{be} = \frac{1}{2} [q_+(\beta) + q_-(\beta)]$, in which $q_+(\beta)$ and $q_-(\beta)$ are probabilities of error when bits “0” and “1” are sent, respectively, i.e.,

$$\begin{aligned}
q_+(\beta) &= \Pr(u > \beta | \text{zero}) \approx \frac{\exp[\Phi_0(s_0)]}{\sqrt{2\pi\Phi_0''(s_0)}}, \\
q_-(\beta) &= \Pr(u \leq \beta | \text{one}) \approx \frac{\exp[\Phi_1(s_1)]}{\sqrt{2\pi\Phi_1''(s_1)}}, \\
\Phi_{b_0}(s) &= \ln[\Psi_{u(b_0)}(s)] - s\beta - \ln|s|, \quad b_0 = 0, 1, \tag{30}
\end{aligned}$$

where u is the photoelectrons count at the receiver output and $\Psi_{u(b_0)}(s)$ is the receiver output moment generating function (MGF) when bit “ b_0 ” is sent. Also s_0 is the positive and real root of $\Phi_0'(s)$, i.e., $\Phi_0'(s_0) = 0$ and s_1 is the negative and real root of $\Phi_1'(s)$, i.e., $\Phi_1'(s_1) = 0$; and β is the receiver optimum threshold and will be chosen such that it minimizes the error probability, i.e., $dP_{be}/d\beta = 0$. As an another approach to evaluate the system BER, Gaussian approximation is very fast and computationally efficient, yet not as accurate as saddle-point approximation, but yields an acceptable estimate of the system error rate particularly for BER values smaller than 0.1

[27]. Indeed, when the receiver output is as $u = N + \xi$, where N is a Poisson distributed RV with mean $m^{(b_0)}$ for transmitted bit “ b_0 ” and ξ is a Gaussian distributed RV with mean zero and variance σ^2 , Gaussian approximation which approximates N as a Gaussian distributed RV with equal mean and variance results to the following equation for the system BER [27];

$$P_{be} = Q \left(\frac{m^{(1)} - m^{(0)}}{\sqrt{m^{(1)} + \sigma^2} + \sqrt{m^{(0)} + \sigma^2}} \right). \quad (31)$$

In this section, the required expressions for both the exact and the upper bound BER evaluations using either saddle-point or Gaussian approximation are presented, when EGC is used at the receiver side.

A. SISO Configuration

In SISO scheme, the photo-detected signal generated by integrate-and-dump circuit can be expressed as;

$$u_{\text{SISO}}^{(b_0)} = y_{\text{SISO}}^{(b_0)} + v_{th}, \quad (32)$$

where v_{th} corresponds to the receiver integrated thermal noise and is a Gaussian distributed RV with mean zero and variance $\sigma_{th}^2 = \frac{2K_b T_r T_b}{R_L q^2}$, where K_b , T_r and R_L are Boltzmann’s constant, the receiver equivalent temperature and load resistance, respectively [30]. Conditioned on $\{b_k\}_{k=-L}^{-1}$ and α , $y_{\text{SISO}}^{(b_0)}$ is a Poisson distributed RV with mean $m_{\text{SISO}}^{(b_0)}$ as;

$$m_{\text{SISO}}^{(b_0)} = \frac{\eta \alpha^2}{hf} \sum_{k=-L}^0 b_k \int_0^{T_b} \Gamma(t - kT_b) dt + (n_b + n_d)T_b, \quad (33)$$

in which n_b and n_d are mean count rates of Poisson distributed background radiation and dark current noise, respectively.

As it is shown in Appendix B, conditioned on α the receiver output MGF can be expressed as;

$$\Psi_{u_{\text{SISO}}^{(b_0)}|\alpha}(s) = \exp \left(\frac{s^2 \sigma_{th}^2}{2} + \left[m_{\text{SISO}}^{(bd)} + b_0 \alpha^2 m^{(s)} \right] (e^s - 1) \right) \times \prod_{k=-L}^{-1} \left[\frac{1 + \exp(\alpha^2 m^{(I,k)} (e^s - 1))}{2} \right], \quad (34)$$

in which $m_{\text{SISO}}^{(bd)} = (n_b + n_d)T_b$, $m^{(s)} = \frac{\eta}{hf} \int_0^{T_b} \Gamma(t) dt$ and $m^{(I,k)} = \frac{\eta}{hf} \int_0^{T_b} \Gamma(t - kT_b) dt = \frac{\eta}{hf} \int_{-kT_b}^{(-k+1)T_b} \Gamma(t) dt$. Moreover, assuming the transmitted data sequences as $b_{k \neq 0} = 1$ for $b_0 = 0$ and $b_{k \neq 0} = 0$ for $b_0 = 1$, MGF of the receiver output for evaluation of upper bound on the BER of SISO-UWOC system can be obtained as;

$$\Psi_{u_{\text{SISO}}^{(b_0)}|\alpha}^{(\text{UB})}(s) = \exp \left(\frac{s^2 \sigma_{th}^2}{2} + \left[m_{\text{SISO}}^{(bd)} + b_0 \alpha^2 m^{(s)} + \sum_{k=-L}^{-1} \bar{b}_0 \alpha^2 m^{(I,k)} \right] (e^s - 1) \right), \quad (35)$$

where $\bar{b}_0 = 1 - b_0$. Inserting (34) and (35) in (30) results into conditional BER, $P_{be|\alpha}$, and the final BER can then be obtained by averaging over fading coefficient α .

B. MIMO Configuration with EGC

In this scheme, each of N receiving apertures receives the sum of all transmitters signals. At the receiver side, each of these N received signals passes through its receiver photodetector and different types of noises are added to each output. Therefore, the photo-detected signal at the j th receiver generated by integrate-and-dump circuit can be expressed as $u_j^{(b_0)} = y_j^{(b_0)} + v_{th,j}$, where $v_{th,j}$ is a Gaussian distributed RV with mean zero and variance $\sigma_{th,j}^2 = \sigma_{th}^2$ corresponding to the integrated thermal noise of the j th receiver and $y_j^{(b_0)}$ conditioned on $\{b_k\}_{k=-L_{ij}}^{-1}$ and $\{\alpha_{ij}\}_{i=1}^M$ is a Poisson distributed RV with mean;

$$m_j^{(b_0)} = \frac{\eta}{hf} \sum_{i=1}^M \sum_{k=-L_{ij}}^0 \alpha_{ij}^2 b_k \int_0^{T_b} \Gamma_{i,j}(t - kT_b) dt + (n_{d,j} + n_{b,j})T_b, \quad (36)$$

where $n_{b,j}$ and $n_{d,j}$ are the mean count rates of Poisson distributed background radiation and dark current noise of the j th receiver, respectively. As it is demonstrated in Appendix C, MGF of the receiver output in MIMO scheme conditioned on fading coefficients vector $\vec{\alpha} = (\alpha_{11}, \alpha_{12}, \dots, \alpha_{MN})$ can be expressed as Eq. (37),² in which $m_{\text{MIMO}}^{(bd)} = (n_b + N n_d)T_b$, $m_{i,j}^{(s)} = \frac{\eta}{hf} \int_0^{T_b} \Gamma_{i,j}(t) dt$ and $m_{i,j}^{(I,k)} = \frac{\eta}{hf} \int_0^{T_b} \Gamma_{i,j}(t - kT_b) dt = \frac{\eta}{hf} \int_{-kT_b}^{(-k+1)T_b} \Gamma_{i,j}(t) dt$. Furthermore, MGF of the receiver output for evaluation of upper bound on the BER of MIMO-UWOC system can be expressed as Eq. (38), shown at the top of the next page.

We should emphasize that extracting the output MGFs for MISO and single-input multiple-output (SIMO) schemes is straightforward by substituting $N = 1$ and $M = 1$, respectively, in (37) and (38).³ Eventually, using saddle-point approximation the conditional BER $P_{be|\vec{\alpha}}$ can be achieved by inserting (37) and (38) in (30). The final BER can then be evaluated by averaging over $\vec{\alpha}$ as $P_{be} = \int_{\vec{\alpha}} P_{be|\vec{\alpha}} f_{\vec{\alpha}}(\vec{\alpha}) d\vec{\alpha}$.

With respect to the above complex expressions, using saddle-point approximation for BER evaluation may be difficult and computationally time-consuming, since it needs to solve some complicated equations for which their complexity increases as ISI (or equivalently L_{\max} in (37)) increases. But (31) suggests that using Gaussian approximation is simple and computationally fast. It can be easily shown that conditioned on b_k the receiver output signal is the sum of a Gaussian and a Poisson RVs; therefore, Gaussian approximation can be applied to evaluate the average BER conditioned on $\vec{\alpha}$ and b_k , i.e., $P_{be|\vec{\alpha}, b_k}$. The Gaussian distributed RV has mean zero and variance $N \sigma_{th}^2$. On the other hand, the Poisson distributed RV has mean $m^{(b_0)}$ which for each of the configurations is as

²Note that each of receivers introduces a Gaussian distributed thermal noise with mean zero and variance $\sigma_{th,j}^2 = \sigma_{th}^2$ and a Poisson distributed dark current with mean count of $n_{d,j}T_b = n_d T_b$. But mean of the Poisson distributed background noise is proportional to the receiver aperture size and we assumed that the sum of all receiving apertures is identical to the aperture size of MISO scheme, which implies that $\sum_{j=1}^N n_{b,j} = n_b$.

³Note that $m_{\text{MISO}}^{(bd)} = m_{\text{SISO}}^{(bd)}$ and $m_{\text{SIMO}}^{(bd)} = m_{\text{MIMO}}^{(bd)}$.

$$\Psi_{u_{\text{MIMO}}^{(b_0)}|\bar{\alpha}}(s) = \exp\left(\frac{N\sigma_{th}^2}{2}s^2 + \left[m_{\text{MIMO}}^{(bd)} + \sum_{j=1}^N \sum_{i=1}^M b_0 \alpha_{ij}^2 m_{i,j}^{(s)}\right](e^s - 1)\right) \times \prod_{j=1}^N \prod_{k=-L_{\max}}^{-1} \frac{1}{2} \left[1 + \prod_{i=1}^M \exp\left(\alpha_{ij}^2 m_{i,j}^{(I,k)}(e^s - 1)\right)\right], \quad (37)$$

$$\Psi_{u_{\text{MIMO}}^{(b_0)}|\bar{\alpha}}(s) = \exp\left(\frac{N\sigma_{th}^2}{2}s^2 + \left[m_{\text{MIMO}}^{(bd)} + \sum_{j=1}^N \sum_{i=1}^M \alpha_{ij}^2 \left(b_0 m_{i,j}^{(s)} + \bar{b}_0 \sum_{k=-L_{ij}}^{-1} m_{i,j}^{(I,k)}\right)\right](e^s - 1)\right). \quad (38)$$

follows;

$$m_{\text{SISO}}^{(b_0)} = m_{\text{SISO}}^{(bd)} + b_0 \alpha^2 m^{(s)} + \sum_{k=-L}^{-1} b_k \alpha^2 m^{(I,k)}, \quad (39)$$

$$m_{\text{MISO}}^{(b_0)} = m_{\text{MISO}}^{(bd)} + \sum_{i=1}^M \left[b_0 \alpha_{i1}^2 m_{i,1}^{(s)} + \sum_{k=-L_{i1}}^{-1} b_k \alpha_{i1}^2 m_{i,1}^{(I,k)} \right], \quad (40)$$

$$m_{\text{SIMO}}^{(b_0)} = m_{\text{SIMO}}^{(bd)} + \sum_{j=1}^N \left[b_0 \alpha_{1j}^2 m_{1,j}^{(s)} + \sum_{k=-L_{1j}}^{-1} b_k \alpha_{1j}^2 m_{1,j}^{(I,k)} \right], \quad (41)$$

$$m_{\text{MIMO}}^{(b_0)} = m_{\text{MIMO}}^{(bd)} + \sum_{j=1}^N \sum_{i=1}^M \left[b_0 \alpha_{ij}^2 m_{i,j}^{(s)} + \sum_{k=-L_{ij}}^{-1} b_k \alpha_{ij}^2 m_{i,j}^{(I,k)} \right]. \quad (42)$$

Moreover, mean of the Poisson distributed RV for evaluation of upper bound on the BER of UWOC system can easily be obtained by assuming the transmitted data sequences as $b_{k \neq 0} = 1$ for $b_0 = 0$ and $b_{k \neq 0} = 0$ for $b_0 = 1$.

Using (31) and (39)-(42) the conditional BER, $P_{be|\bar{\alpha}, b_k}$, can easily be evaluated based on Gaussian approximation. Moreover, to obtain $P_{be|\bar{\alpha}, b_k}$ based on saddle-point approximation the simplified form of saddle-point approximation [27, Eqs. (5.73)-(5.79)] can be applied to (39)-(42). Subsequently, $P_{be|b_k}$ can be obtained through an $(M \times N)$ -dimensional integration as $P_{be|b_k} = \int_{\bar{\alpha}} P_{be|\bar{\alpha}, b_k} f_{\bar{\alpha}}(\bar{\alpha}) d\bar{\alpha}$ which yet demands excessive computational time, especially for large number of links. Nevertheless, we can reformulate (42) as $m_{\text{MIMO}}^{(b_0)} = m_{\text{MIMO}}^{(bd)} + \sum_{j=1}^N \sum_{i=1}^M \left[\tau_{i,j}^{(b_0)} \alpha_{ij}^2 \right]$, where $\tau_{i,j}^{(b_0)} = b_0 m_{i,j}^{(s)} + \sum_{k=-L_{ij}}^{-1} b_k m_{i,j}^{(I,k)}$. Hence, we can approximate (42) as $m_{\text{MIMO}}^{(b_0)} \approx \tilde{m}_{\text{MIMO}}^{(b_0)} = m_{\text{MIMO}}^{(bd)} + \vartheta^{(b_0)}$, where $\tilde{m}_{\text{MIMO}}^{(b_0)}$ is the approximated version of (42) and $\vartheta^{(b_0)} \approx \sum_{j=1}^N \sum_{i=1}^M \tau_{i,j}^{(b_0)} \alpha_{ij}^2$, i.e., the weighted sum of $M \times N$ RVs. In the special case of weak oceanic turbulence the equivalent log-normal RV, $\vartheta^{(b_0)} = \exp(2z^{(b_0)})$, has the following log-amplitude mean and variance, respectively [23];

$$\mu_{z^{(b_0)}} = \frac{1}{2} \ln \left(\sum_{j=1}^N \sum_{i=1}^M \tau_{i,j}^{(b_0)} \right) - \sigma_{z^{(b_0)}}^2, \quad (43)$$

$$\sigma_{z^{(b_0)}}^2 = \frac{1}{4} \ln \left(1 + \frac{\sum_{j=1}^N \sum_{i=1}^M \left(\tau_{i,j}^{(b_0)} \right)^2 \left(e^{4\sigma_{x_{ij}}^2} - 1 \right)}{\left(\sum_{j=1}^N \sum_{i=1}^M \tau_{i,j}^{(b_0)} \right)^2} \right). \quad (44)$$

By means of the above approximation $P_{be|b_k}$ can be evaluated through two-dimensional integral of $P_{be|b_k} \approx \int_0^\infty \int_0^\infty P_{be|b_k, \vartheta^{(0)}, \vartheta^{(1)}} f(\vartheta^{(0)}, \vartheta^{(1)}) d\vartheta^{(0)} d\vartheta^{(1)}$, where $P_{be|b_k, \vartheta^{(0)}, \vartheta^{(1)}}$ is the average BER of the system conditioned on b_k , $\vartheta^{(0)}$ and $\vartheta^{(1)}$, and (when Gaussian approximation is used) is defined as;

$$P_{be|b_k, \vartheta^{(0)}, \vartheta^{(1)}} \approx Q \left(\frac{\tilde{m}_{\text{MIMO}}^{(1)} - \tilde{m}_{\text{MIMO}}^{(0)}}{\sqrt{\tilde{m}_{\text{MIMO}}^{(1)} + N\sigma_{th}^2} + \sqrt{\tilde{m}_{\text{MIMO}}^{(0)} + N\sigma_{th}^2}} \right). \quad (45)$$

It is worth mentioning that in the MISO scheme all the transmitters are pointed to a single receiver; therefore, all the links have the same fading-free impulse response and channel memory as $h_{0,\text{MISO}}(t)$ and L_{MISO} , respectively. Consequently, when all transmitters have identical transmit power of P/M , all links have equal $m_{i,1}^{(s)}$ and $m_{i,1}^{(I,k)}$ as $m_{\text{MISO}}^{(s)}$ and $m_{\text{MISO}}^{(I,k)}$, respectively. Hence, we can rewrite (40) as $m_{\text{MISO}}^{(b_0)} = m_{\text{MISO}}^{(bd)} + \left(b_0 m_{\text{MISO}}^{(s)} + \sum_{k=-L_{\text{MISO}}}^{-1} b_k m_{\text{MISO}}^{(I,k)} \right) \varphi^{(M)}$, where $\varphi^{(M)} = \sum_{i=1}^M \alpha_{i1}^2$, i.e., the sum of M log-normal RVs. As a result, $P_{be|b_k}$ for MISO scheme can be evaluated through one-dimensional integral of $P_{be|b_k} \approx \int_0^\infty P_{be|b_k, \varphi^{(M)}} f(\varphi^{(M)}) d\varphi^{(M)}$. Then, if the channel memory is L_{\max} bits, P_{be} can be obtained by averaging as $P_{be} = \frac{1}{2^{L_{\max}}} \sum_{b_k} P_{be|b_k}$. Note that as ISI increases, this averaging demands more computational time and evaluation of the upper bound BER becomes more advantageous.

From Eqs. (39)-(42), one can observe the destructive effect of ISI on the BER. In other words, experiencing more time spreading in $h_{0,ij}(t)$ or equivalently $\Gamma_{i,j}(t)$ increases $\sum_{k \neq 0} m_{i,j}^{(I,k)}$ and decreases $m_{i,j}^{(s)}$. Thereby, it causes an increase in $m^{(0)}$ and a decrease in $m^{(1)}$ which results in higher BER. Constructive effect of spatial diversity is appeared as combining the fading coefficients of different links which can be approximated as a single log-normal RV with roughly a scaled log-amplitude variance by the number of links [9].

V. NUMERICAL RESULTS

In this section, we present numerical results for the BER performance of UWOC systems in various scenarios. We consider log-normal distribution for the channel fading statistics, equal power as P/M for all transmitters, same fading statistics (log-amplitude variance) for all links and the same aperture area of A/N for all of the receivers, where A is the total aperture area. In simulating the turbulence-free impulse

TABLE I
SOME OF THE IMPORTANT PARAMETERS USED FOR NOISE
CHARACTERIZATION AND MC-BASED CHANNEL SIMULATION.

Coefficient	Value
Quantum efficiency, η	0.8
Optical filter bandwidth, $\Delta\lambda$	10 nm
Optical filter transmissivity, T_F	0.8
Equivalent temperature, T_e	290 K
Load resistance, R_L	100 Ω
Dark current, I_{dc}	1.226×10^{-9} A
Receiver half angle FOV, θ_{FOV}	40°
MISO schemes aperture diameter, $D_0^{(MISO)}$	20 cm
Source wavelength, λ	532 nm
Water refractive index, n	1.331
Source full beam divergence angle, θ_{div}	0.02°
Photon weight threshold at the receiver, w_{th}	10^{-6}
Separation distance between the transmitters and between the receiving apertures, l_0	25 cm

response by MC method we consider coastal water link which has $a = 0.179 \text{ m}^{-1}$, $b = 0.219 \text{ m}^{-1}$ and $c = 0.398 \text{ m}^{-1}$ [3]. Other important parameters for MC simulations are listed in Table I. In addition, some of the important parameters for characterization of noises are addressed in this table and the other parameters are exactly the same as those mentioned in [6], [31]. Based on these parameters, noise characteristics are as $n_b \approx 1.8094 \times 10^8 \text{ s}^{-1}$ in 30 meters deep ocean, $n_d \approx 76.625 \times 10^8 \text{ s}^{-1}$, and $\sigma_{th}^2/T_b = 3.12 \times 10^{15} \text{ s}^{-1}$. Hence, background radiation has a negligible effect on the system performance.

Fig. 2 depicts the exact BER of a 25 m coastal water link with transmitter diversity and data transmission rate of $R_b = 1$ Gbps. This figure also indicates excellent matches between the results of analytical expressions and numerical simulations. We assume that the fading of each link is independent from the others. As it is obvious, increasing the number of independent links provides significant performance improvement in the case of $\sigma_X = 0.4$, e.g., one can achieve approximately 6 dB and 9 dB performance improvement at the BER of 10^{-12} , using two and three transmitters, respectively. But this benefit relatively vanishes in very weak fading conditions, e.g., $\sigma_X = 0.1$. This is reasonable, since in very weak turbulence conditions fading has a minuscule effect on the performance, but scattering and absorption have yet substantial effects. Hence, in such scenarios multiple transmitters scheme which combats with impairing effects of fading does not provide notable performance improvement.

In Fig. 3, we assume the same parameters as in Fig. 2 and use our derived analytical expressions to evaluate the exact BER of 1×2 SIMO, 1×3 SIMO and 2×2 MIMO configurations with optimal/equal gain combiner. Comparison between the results show that the performance of EGC is very close to the performance of OC receiver. Therefore, due to its lower complexity, receiver with EGC is more practically interesting. Furthermore, well matches between the analytical results and numerical simulations confirm the accuracy of our derived analytical expressions for the system BER. Moreover, it is observed that in the case of $\sigma_X = 0.4$, 1×3 SIMO scheme provides better performance than 1×2 SIMO only at

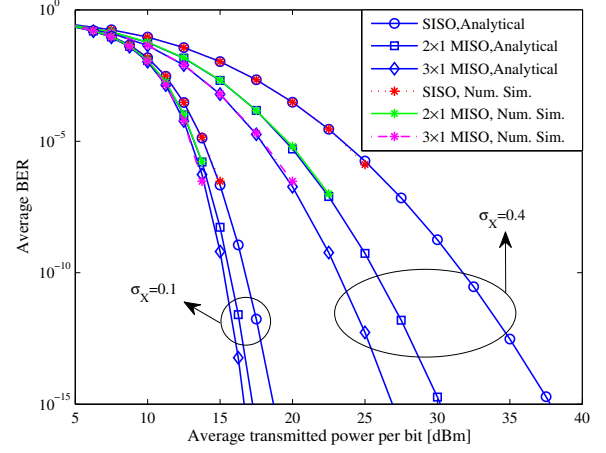


Fig. 2. Exact BER of a 25 m coastal water link with SISO, 2×1 MISO and 3×1 MISO configurations, obtained using both analytical expressions and numerical simulations. $R_b = 1$ Gbps, $\sigma_X = 0.1$ and 0.4 .

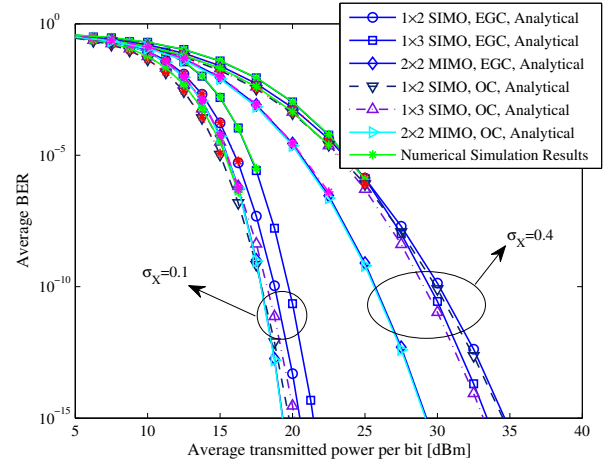


Fig. 3. Exact BER of a 25 m coastal water link with 1×2 SIMO, 1×3 SIMO and 2×2 MIMO configurations and optimal/equal gain combiner, obtained using both analytical expressions and numerical simulations. $R_b = 1$ Gbps, $\sigma_X = 0.1$ and 0.4 .

high signal-to-noise ratios (SNRs) or equivalently low BERs, where fading has more impairing effect than absorption and ISI. This is reasonable, since each receiver in 1×3 SIMO scheme has 1.5 times less aperture area than in 1×2 SIMO and also 3-receiver scheme imposes 1.5 times more dark current and thermal noise. In low SNRs, absorption and scattering as well as noise have more dominant effects on the BER than fading; therefore, in low SNRs 1×2 SIMO scheme yields better performance than 1×3 SIMO structure. But since channel suffers from relatively notable turbulence, 1×3 SIMO structure which has more links can make better fading mitigation and can compensate for the loss due to smaller aperture size and excess noise and therefore can yield better performance at higher SNRs. Needless to say that 2×2 MIMO structure has the same aperture size as 1×2 SIMO structure and since benefits from more independent links can yield better performance in all ranges of SNR. One can expect that in a

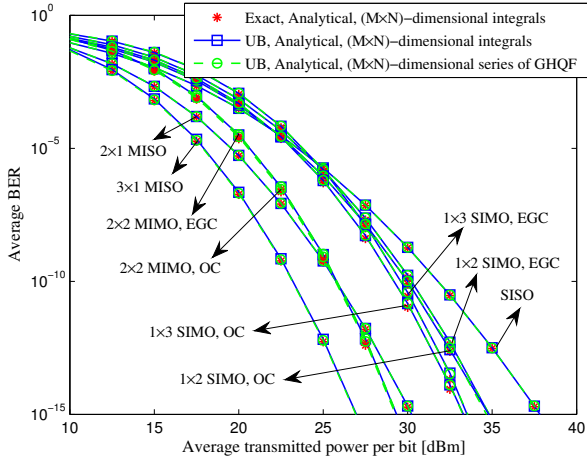


Fig. 4. Comparison between the exact and the upper bound BERs of a 25 m coastal water link with $R_b = 1$ Gbps, $\sigma_X = 0.4$, and various configurations. Also the upper bound BERs are calculated with $(M \times N)$ -dimensional series, using Gauss-Hermite quadrature formula (GHQF).

very weak turbulence scenario, such as $\sigma_X = 0.1$, dividing the receiver aperture to extend the number of independent links can degrade the performance.

In Fig. 4 we applied our derived analytical expressions to evaluate the exact and the upper bound BERs of a 25 m coastal water link with $R_b = 1$ Gbps and $\sigma_X = 0.4$, using $(M \times N)$ -dimensional integrals. As it can be seen, the upper bound BER curves have well tightness with the exact BER curves. Therefore, the upper bound BER evaluation can be more preferable, since the exact BER calculation may need excessive time for averaging over b_k s. Furthermore, the upper bound BERs of various configurations are calculated by $(M \times N)$ -dimensional series, using Gauss-Hermite quadrature formula (GHQF). The order of approximation U is assumed to be the same for all of the links, i.e., $U_{ij} = 30$. Excellent matches between the results of GHQF and numerical $(M \times N)$ -dimensional integrals demonstrate the usefulness of GHQF in effective calculation of the system BER.

Fig. 5 compares Gaussian and saddle-point approximations in evaluating the exact BER of a 25 m coastal water link with $R_b = 1$ Gbps, $\sigma_X = 0.4$, and various configurations. It is observed that Gaussian approximation can provide relatively the same results as saddle-point approximation. Therefore, due to its simplicity and acceptable accuracy, Gaussian approximation can be considered as a reliable photon-counting method for the system BER evaluation. Moreover, the results of our derived analytical expressions are compared with those of photon-counting methods. Well matches between the results of analytical expressions and photon-counting methods further confirm the validity of our assumption in neglecting the signal-dependent shot noise for our analytical derivations.

In Fig. 6 the BER performance of a 25 m coastal water link with $R_b = 0.5$ Gbps and $\sigma_X = 0.3$ is depicted for different configurations. Also the sum of independent log-normal RVs in (40)-(42) is approximated with a single log-normal RV and the BER is evaluated through the approximated one-or two-dimensional integrals. As it can be seen, relatively well

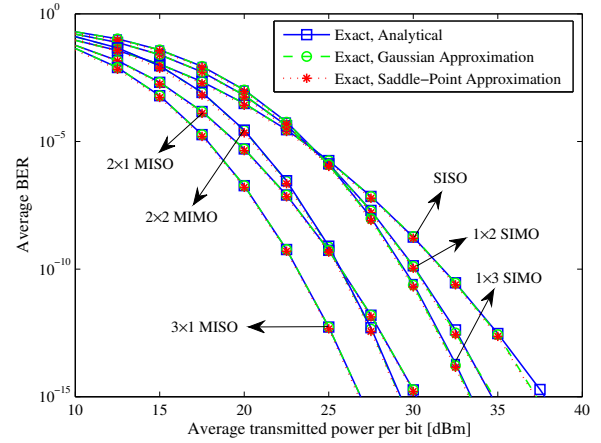


Fig. 5. Comparing Gaussian and saddle-point approximations in evaluating the exact BER of a 25 m coastal water link with $R_b = 1$ Gbps, $\sigma_X = 0.4$, and various configurations. Also the results of photon-counting methods are compared with the results of our derived analytical expressions for the system exact BER.

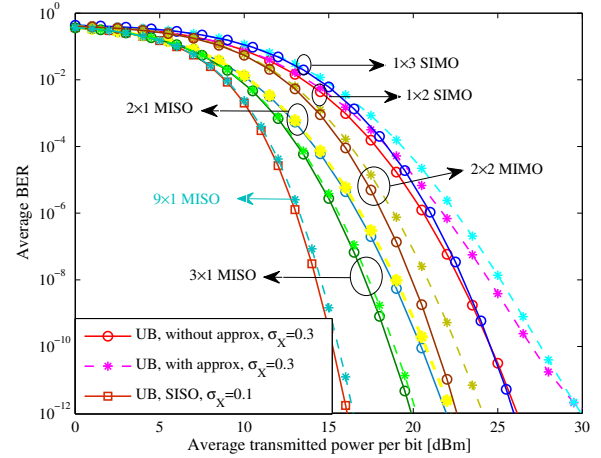


Fig. 6. Upper bound and approximated upper bound on the BER of a 25 m coastal water link with different configurations, obtained using Gaussian approximation. $R_b = 0.5$ Gbps, $\sigma_X = 0.3$ and 0.1 .

match exists between results of the approximated one-or two-dimensional integrals and the exact $(M \times N)$ -dimensional integral of $P_{be} = \int_{\vec{\alpha}} P_{be|\vec{\alpha}} f_{\vec{\alpha}}(\vec{\alpha}) d\vec{\alpha}$. However, the discrepancy increases when receiver diversity is used. Moreover, the BER performance of a SISO link with $\sigma_X = 0.1$ is compared with the BER curve of a 9×1 MISO link with $\sigma_X = 0.3$, and approximately the same result is observed; therefore, spatial diversity manifests its effect as a reduction in fading log-amplitude variance.

In order to see the destructive effect of ISI, in Fig. 7 upper bound on the BER of a 25 m coastal water link with $\sigma_X = 0.4$ and various configurations is illustrated for two different data rates, namely 0.5 Gbps and 50 Gbps, and considerable degradation is observed. As it can be seen, in relatively low data rates spatial diversity can introduce remarkable performance improvement, especially for multiple transmitters schemes. But at high data rates receiver diversity

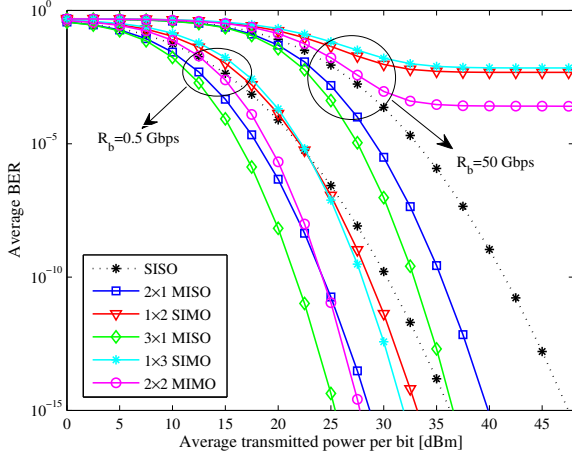


Fig. 7. Effect of ISI on the performance of a 25 m coastal water link with different configurations. $\sigma_X = 0.4$, $R_b = 0.5$ Gbps and 50 Gbps.

degrades the performance, particularly at high SNR regimes. However, transmitter diversity yet results a noticeable performance improvement. This is reasonable, since in our system model all the transmitters of the MISO scheme are pointed to a single receiver. In other words, the receiver only receives those photons that have experienced a little scattering. On the other hand, In SIMO scheme the transmitter is pointed to one of the receivers and therefore, the other receivers capture those photons that have experienced a remarkable scattering. This contribution to the received optical signal can introduce a notable ISI, especially for high data rates. Furthermore, in the MIMO scheme each receiving aperture in addition to receiving photons from the transmitter that is pointed to this aperture, receives the other transmitters' scattered photons.

Fig. 8 indicates the channel impulse responses of a 25 m coastal water link with 1×2 SIMO structure. The transmitter is pointed to the first receiver and the link between the transmitter and the first receiver has the impulse response of $h_{0,11}(t)$. The second receiver is located 25 cm away from the first receiver. This receiver receives those photons that are reached to its aperture with scattering; with impulse response of $h_{0,12}(t)$. Each receiving aperture has a diameter of $20/\sqrt{2}$ cm. As it can be seen, $h_{0,11}(t)$ has a negligible scattering; however, $h_{0,12}(t)$ imposes a notable time spreading on the total received optical signal. It should be noted that decreasing the separation distance between the receiving apertures alleviates this time spreading, but this approach increases the spatial correlation between different links' signal, which degrades the system performance (as it is shown in Fig. 10). On the other hand, we can reduce the ISI effect by decreasing the receiver aperture size, but this scheme induces more loss on the received optical signal.

Fig. 9 illustrates the main purpose of this paper. In this figure we want to show that although increasing the communication distance increases absorption (loss), scattering (ISI) and turbulence (fading), yet using spatial diversity one can achieve better performance than SISO links with smaller distances and therefore can increase the viable communication range.

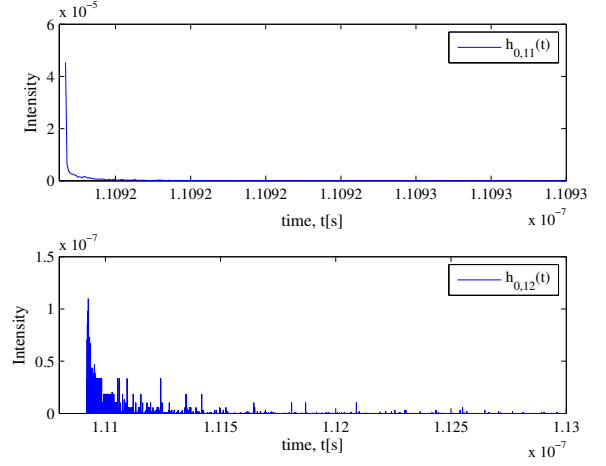


Fig. 8. Channel fading-free impulse responses of a 25 m coastal water link with 1×2 SIMO structure.

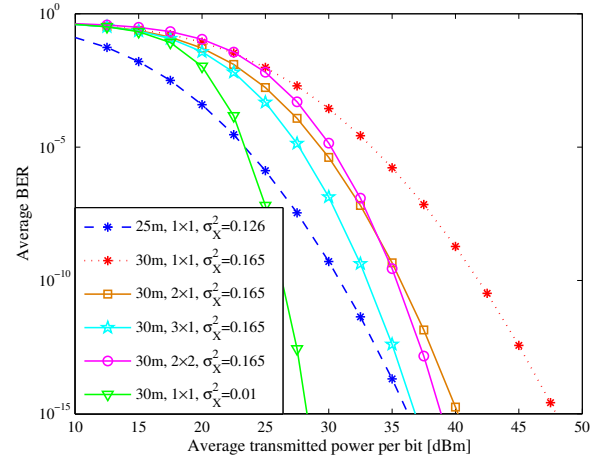


Fig. 9. Comparison between the performance of a 30 m coastal water link with different configurations and a 25 m SISO link, both operating at $R_b = 2$ Gbps.

To show that, we consider a coastal water with scintillation parameters of $\varepsilon = 10^{-5} \text{ m}^2/\text{s}^3$, $w = -3$ and $\chi_T = 4 \times 10^{-7} \text{ K}^2/\text{s}$, and numerically evaluate Eq. (3) to find the scintillation index of a plane wave for different link ranges. Based on our numerical results we find that for $d_0 = 25$ m and 30 m the log-amplitude variance σ_X^2 is 0.126 and 0.165, respectively. As it is obvious in this figure, only 5 m (%20) increase on the communication range remarkably degrades the system performance, e.g., approximately 12 dB degradation is observed at the BER of 10^{-12} . But as it can be seen, increasing the number of independent links or equivalently mitigating fading deteriorations considerably improves the system performance. Since spatial diversity manifests itself as a reduction in fading variance [9], we can conclude that there exists a configuration with spatial diversity at link range of 30 m which performs similar to a SISO link at that range but with less fading variance, e.g., $\sigma_X^2 = 0.01$. Hence, in this figure the performance of a 30 m SISO link with $\sigma_X^2 = 0.01$ is also depicted for the sake of comparison and obviously

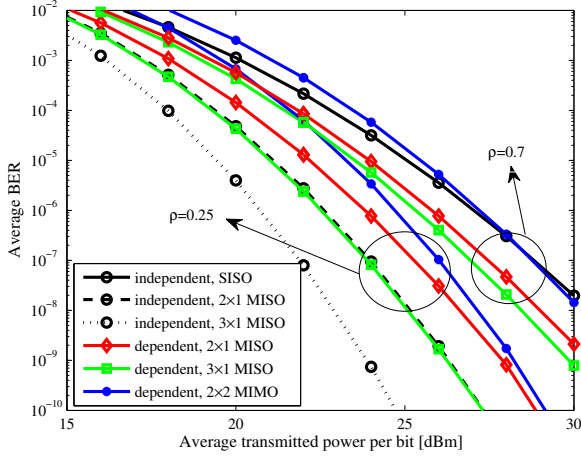


Fig. 10. Effect of spatial correlation on the performance of a 25 m coastal water link with $\sigma_X = 0.4$, $R_b = 2$ Gbps, $\rho = 0.25$ and 0.7 .

it can yield better performance than a 25 m SISO link, especially for lower error rates. Therefore, one can achieve better performance even in longer link ranges by employing spatial diversity technique. We should emphasize that spatial diversity can provide more performance enhancement rather than those are presented in this paper; when the channel suffers from strong turbulence [12]. But since this paper is focused on weak oceanic turbulence, we only considered channels with $\sigma_I^2 < 1$ [10].

As observed, spatial diversity provides a significant performance improvement but under the assumption of independent links which is sometimes practically infeasible [32]. Therefore, in practice received signals by different links may have correlation. In Fig. 10 the effect of spatial correlation on the performance of an UWOC link is investigated in similar approach to [9]. We considered a 25 m coastal water link with $\sigma_X = 0.4$ and $R_b = 2$ Gbps, and evaluated the upper bound BER of different configurations in several cases, i.e., independent links and correlated links with correlation values of $b(l_0) = \rho = 0.25$ and 0.7 . Comparing the results shows that the performance loss is much more severe for larger correlation values, e.g., 2 dB and 6 dB degradation can be observed in the performance of a 3×1 MISO link with the BER of 10^{-10} and with $\rho = 0.25$ and 0.7 , respectively. Also a 3×1 MISO link with $\rho = 0.25$ yields the same performance as an independent 2×1 MISO link, i.e., diversity order is decreased by one. Therefore, performance enhancement by spatial diversity can be minuscule in highly correlated weak turbulent channels.

VI. CONCLUSION

In this paper, we studied the performance of MIMO-UWOC systems with OOK modulation and equal gain or optimal combiner. Closed-form solutions for the system BER expressions obtained in the case of log-normal underwater fading channels, relying on Gauss-Hermite quadrature formula as well as approximation to the sum of log-normal random variables. We also applied photon-counting method to evaluate the system BER in the presence of shot noise. Well matches

between the results of analytical expressions and photon-counting method confirmed the validity of our assumptions in derivation of analytical expressions for the system BER. Furthermore, our numerical results indicated that EGC is more practically interesting, due to its lower complexity and its similar performance to optimal combiner. In addition to evaluating the exact BER, also the upper bound on the system BER evaluated and excellent tightness between the exact and the upper bound BER curves observed. Moreover, well matches between the results of numerical simulations and analytical expressions verified the accuracy of our derived analytical expressions for the system BER. Our numerical results showed that spatial diversity manifests its effect as a reduction in fading variance and hence can significantly improve the system performance and increase the viable communication range. In particular, a 3×1 MISO transmission in a 25 m coastal water link with log-amplitude variance of 0.16 can introduce 8 dB performance improvement at the BER of 10^{-9} . We also observed that spatial correlation can impose a severe loss on the performance of MIMO system. Specifically, correlation value of $\rho = 0.25$ between the links of a 3×1 MISO UWOC system with $\sigma_X = 0.4$ decreases the order of diversity by one. Finally, we should emphasize that although all the numerical results of this paper are based on log-normal distribution, many of our derivations can be used for any other fading statistical distribution.

APPENDIX A

$(M \times N)$ -DIMENSIONAL SERIES OF GAUSS-HERMITE QUADRATURE FORMULA

In this appendix, we show how $(M \times N)$ -dimensional averaging integrals over fading coefficients can effectively be calculated using Gauss-Hermite quadrature formula [28, Eq. (25.4.46)]. More specifically we calculate $P_{be|b_0, b_k}^{(MIMO)} = \int_{\vec{\alpha}} P_{be|b_0, \vec{\alpha}, b_k}^{(MIMO)} f_{\vec{\alpha}}(\vec{\alpha}) d\vec{\alpha}$ with $(M \times N)$ -dimensional series, where $P_{be|b_0, \vec{\alpha}, b_k}^{(MIMO)}$ is defined in (19) and (20) for $b_0 = 1$ and $b_0 = 0$, respectively. Based on (13) and [28, Eq. (25.4.46)], for any function $g(\alpha_{ij}^2)$ averaging over log-normal distributed fading coefficient α_{ij} can be calculated with a finite series as;

$$\int_0^\infty g(\alpha_{ij}^2) f_{\alpha_{ij}}(\alpha_{ij}) d\alpha_{ij} \approx \frac{1}{\sqrt{\pi}} \sum_{q_{ij}=1}^{U_{ij}} w_{q_{ij}}^{(ij)} g(\alpha_{ij}^2 = \exp(2x_{q_{ij}}^{(ij)} \sqrt{2\sigma_{X_{ij}}^2} + 2\mu_{X_{ij}})) \quad (46)$$

Further, the validity of Eq. (47), shown at the top of the next page, can be verified by induction for any function of $M \times N$ log-normal distributed fading coefficients $g(\alpha_{11}^2, \alpha_{21}^2, \dots, \alpha_{MN}^2)$. Therefore, the $(M \times N)$ -dimensional integral of $\int_{\vec{\alpha}} P_{be|b_0, \vec{\alpha}, b_k}^{(MIMO)} f_{\vec{\alpha}}(\vec{\alpha}) d\vec{\alpha}$ can be calculated as Eq. (48).

APPENDIX B

MGF OF THE RECEIVER OUTPUT IN SISO SCHEME

In this appendix, we calculate the receiver output MGF in SISO scheme. Based on (32), conditioned on $\{b_k\}_{k=-L}^{-1}$ and α ,

$$\begin{aligned}
& \int_{\alpha_{11}=0}^{\infty} \int_{\alpha_{21}=0}^{\infty} \dots \int_{\alpha_{MN}=0}^{\infty} g(\alpha_{11}^2, \alpha_{21}^2, \dots, \alpha_{MN}^2) f_{\alpha_{11}}(\alpha_{11}) f_{\alpha_{21}}(\alpha_{21}) \dots f_{\alpha_{MN}}(\alpha_{MN}) d\alpha_{11} d\alpha_{21} \dots d\alpha_{MN} \\
& \approx \frac{1}{\pi^{M \times N/2}} \sum_{q_{11}=1}^{U_{11}} w_{q_{11}}^{(11)} \sum_{q_{21}=1}^{U_{21}} w_{q_{21}}^{(21)} \dots \sum_{q_{MN}=1}^{U_{MN}} w_{q_{MN}}^{(MN)} g\left(\alpha_{11}^2 = \exp\left(2x_{q_{11}}^{(11)} \sqrt{2\sigma_{X_{11}}^2} + 2\mu_{X_{11}}\right), \right. \\
& \quad \left. \alpha_{21}^2 = \exp\left(2x_{q_{21}}^{(21)} \sqrt{2\sigma_{X_{21}}^2} + 2\mu_{X_{21}}\right), \dots, \alpha_{MN}^2 = \exp\left(2x_{q_{MN}}^{(MN)} \sqrt{2\sigma_{X_{MN}}^2} + 2\mu_{X_{MN}}\right)\right). \quad (47)
\end{aligned}$$

$$\begin{aligned}
P_{be|b_0, b_k}^{(\text{MIMO})} &= \int_{\vec{\alpha}} P_{be|b_0, \vec{\alpha}, b_k}^{(\text{MIMO})} f_{\vec{\alpha}}(\vec{\alpha}) d\vec{\alpha} \approx \frac{1}{\pi^{M \times N/2}} \sum_{q_{11}=1}^{U_{11}} w_{q_{11}}^{(11)} \sum_{q_{21}=1}^{U_{21}} w_{q_{21}}^{(21)} \dots \sum_{q_{MN}=1}^{U_{MN}} w_{q_{MN}}^{(MN)} \times \\
Q &\left(\frac{\sum_{j=1}^N \sum_{i'=1}^M \gamma_{i',j}^{(s)} \exp\left(2x_{q_{i'j}}^{(i'j)} \sqrt{2\sigma_{X_{i'j}}^2} + 2\mu_{X_{i'j}}\right) \sum_{i=1}^M \left(\gamma_{i,j}^{(s)} + (-1)^{b_0+1} \sum_{k=-L_{ij}}^{-1} 2b_k \gamma_{i,j}^{(I,k)} \right) \exp\left(2x_{q_{ij}}^{(ij)} \sqrt{2\sigma_{X_{ij}}^2} + 2\mu_{X_{ij}}\right)}{2\sigma_{T_b} \sqrt{\sum_{j=1}^N \left(\sum_{i=1}^M \gamma_{i,j}^{(s)} \exp\left(2x_{q_{ij}}^{(ij)} \sqrt{2\sigma_{X_{ij}}^2} + 2\mu_{X_{ij}}\right) \right)^2}} \right). \quad (48)
\end{aligned}$$

$u_{\text{SISO}}^{(b_0)}$ is the sum of two independent RVs. Therefore its MGF $\Psi_{u_{\text{SISO}}^{(b_0)}}(s)$ is the product of their MGFs, i.e., $\Psi_{u_{\text{SISO}}^{(b_0)}}(s) = \Psi_{y_{\text{SISO}}^{(b_0)}}(s) \times \Psi_{v_{th}}(s)$. We first compute the conditional MGF of $y_{\text{SISO}}^{(b_0)}$ conditioned on $\{b_k\}_{k=-L}^{-1}$ and α . Then averaging over $\{b_k\}_{k=-L}^{-1}$ results the MGF of $y_{\text{SISO}}^{(b_0)}$ conditioned on α [27] as Eq. (49), shown at the top of the next page. Note that b_k s are independent Bernoulli RVs with identical probability, i.e.,

$$P_{b_k}(b_k) = \frac{1}{2}\delta(b_k) + \frac{1}{2}\delta(b_k - 1), \quad (50)$$

where $\delta(\cdot)$ is Dirac delta function. Therefore, the latter expectation in (49) simplifies to;

$$\begin{aligned}
& \mathbb{E}_{b_k} \left[\prod_{k=-L}^{-1} \exp\left(b_k \alpha^2 m^{(I,k)} (e^s - 1)\right) \middle| \alpha \right] \\
&= \prod_{k=-L}^{-1} \mathbb{E}_{b_k} \left[\exp\left(b_k \alpha^2 m^{(I,k)} (e^s - 1)\right) \middle| \alpha \right] \\
&= \prod_{k=-L}^{-1} (1/2) \left[1 + \exp\left(\alpha^2 m^{(I,k)} (e^s - 1)\right) \right]. \quad (51)
\end{aligned}$$

Finally, inserting (51) in (49) and then multiplying the result by $\Psi_{v_{th}}(s) = \exp(s^2 \sigma_{th}^2 / 2)$ yields the output MGF as in Eq. (34).

APPENDIX C

MGF OF THE RECEIVER OUTPUT IN MIMO SCHEME

In this appendix, we calculate the MGF of the receiver output in MIMO scheme. Since EGC is used, the combined output of the receiver is $u_{\text{MIMO}}^{(b_0)} = \sum_{j=1}^N u_j^{(b_0)}$. Conditioned on fading coefficients vector $\vec{\alpha}$, received signals from different branches are independent and hence MGF of their sum is the product of each branch's MGF, i.e., $\Psi_{u_{\text{MIMO}}^{(b_0)}|\vec{\alpha}}(s) = \prod_{j=1}^N \Psi_{u_j^{(b_0)}|\{\alpha_{ij}\}_{i=1}^M}(s)$. Therefore, we first need to obtain the conditional MGF of each branch. By pursuing similar steps as in Appendix B, $\Psi_{u_j^{(b_0)}|\{\alpha_{ij}\}_{i=1}^M}(s)$ can be calculated

as Eq. (52), shown at the top of the next page. where $m_j^{(bd)} = (n_{bj} + n_{dj})T_b$. Supposing the same channel memory⁴ as $L_{ij} = L_{\max}$ for all links, performing the latter expectation in (52) results the j th receiver output MGF as;

$$\begin{aligned}
\Psi_{u_j^{(b_0)}|\{\alpha_{ij}\}_{i=1}^M}(s) &= \exp\left(\frac{\sigma_{th}^2 s^2}{2} + \left[m_j^{(bd)} + \sum_{i=1}^M b_0 \alpha_{ij}^2 m_{i,j}^{(s)}\right] (e^s - 1)\right) \\
&\times \prod_{k=-L_{\max}}^{-1} (1/2) \left[1 + \prod_{i=1}^M \exp\left(\alpha_{ij}^2 m_{i,j}^{(I,k)} (e^s - 1)\right) \right]. \quad (53)
\end{aligned}$$

Finally, MGF of the receiver output in MIMO scheme can be obtained as in Eq. (37).

ACKNOWLEDGMENT

The authors would like to thank Mr. Farhad Akhondi for his helpful comments.

REFERENCES

- [1] S. Tang, Y. Dong, and X. Zhang, "Impulse response modeling for underwater wireless optical communication links," *IEEE Trans. Commun.*, vol. 62, no. 1, pp. 226–234, 2014.
- [2] F. Hanson and S. Radic, "High bandwidth underwater optical communication," *Applied optics*, vol. 47, no. 2, pp. 277–283, 2008.
- [3] C. D. Mobley, *Light and water: Radiative transfer in natural waters*. Academic press, 1994.
- [4] V.V. Nikishov and V.I. Nikishov, "Spectrum of turbulent fluctuations of the sea-water refraction index," *Int. J. Fluid Mech. Research*, vol. 27, no. 1, 2000.
- [5] T. J. Petzold, "Volume scattering functions for selected ocean waters," DTIC Document, Tech. Rep., 1972.
- [6] S. Jaruwatanadilok, "Underwater wireless optical communication channel modeling and performance evaluation using vector radiative transfer theory," *IEEE J. Select. Areas Commun.*, vol. 26, no. 9, pp. 1620–1627, 2008.

⁴Note that if some of the links have smaller memory, we can add adequate zero component to each of them in order to make all the links with equal memory length. In other words, if $L_{ij} < L_{\max}$ then $\{m_{i,j}^{(I,k)}\}_{k=-L_{ij}^{-1}}^{-L_{\max}} = 0$.

$$\begin{aligned}\Psi_{y_{\text{SISO}}|_{\alpha}}(s) &= \mathbb{E}_{b_k} \left[e^{m_{\text{SISO}}^{(b_0)}(e^s - 1)} | \alpha \right] = \mathbb{E}_{b_k} \left[\exp \left(\left\{ m_{\text{SISO}}^{(bd)} + b_0 \alpha^2 m^{(s)} + \sum_{k=-L}^{-1} b_k \alpha^2 m^{(I,k)} \right\} (e^s - 1) \right) | \alpha \right] \\ &= \exp \left(\left(m_{\text{SISO}}^{(bd)} + b_0 \alpha^2 m^{(s)} \right) (e^s - 1) \right) \times \mathbb{E}_{b_k} \left[\prod_{k=-L}^{-1} \exp \left(b_k \alpha^2 m^{(I,k)} (e^s - 1) \right) | \alpha \right].\end{aligned}\quad (49)$$

$$\begin{aligned}\Psi_{u_j^{(b_0)} | \{\alpha_{ij}\}_{i=1}^M}(s) &= \exp \left(\frac{\sigma_{th}^2}{2} s^2 \right) \times \mathbb{E}_{b_k} \left[\exp \left(\left\{ m_j^{(bd)} + \sum_{i=1}^M \left[b_0 \alpha_{ij}^2 m_{i,j}^{(s)} + \sum_{k=-L_{ij}}^{-1} b_k \alpha_{ij}^2 m_{i,j}^{(I,k)} \right] \right\} (e^s - 1) \right) | \{\alpha_{ij}\}_{i=1}^M \right] \\ &= \exp \left(\frac{\sigma_{th}^2}{2} s^2 + \left[m_j^{(bd)} + \sum_{i=1}^M b_0 \alpha_{ij}^2 m_{i,j}^{(s)} \right] (e^s - 1) \right) \times \mathbb{E}_{b_k} \left[\prod_{i=1}^M \prod_{k=-L_{ij}}^{-1} \exp \left(b_k \alpha_{ij}^2 m_{i,j}^{(I,k)} (e^s - 1) \right) | \{\alpha_{ij}\}_{i=1}^M \right],\end{aligned}\quad (52)$$

- [7] F. Akhouri, J. A. Salehi, and A. Tashakori, "Cellular underwater wireless optical CDMA network: Performance analysis and implementation concepts," *IEEE Trans. Commun.*, vol. 63, no. 3, pp. 882–891, 2015.
- [8] S. Tang, X. Zhang, and Y. Dong, "Temporal statistics of irradiance in moving turbulent ocean," in *OCEANS-Bergen, 2013 MTS/IEEE*. IEEE, 2013, pp. 1–4.
- [9] S. M. Navidpour, M. Uysal, and M. Kavehrad, "BER performance of free-space optical transmission with spatial diversity," *IEEE Trans. Wireless Commun.*, vol. 6, no. 8, pp. 2813–2819, 2007.
- [10] L. C. Andrews, R. L. Phillips, and C. Y. Hopen, *Laser beam scintillation with applications*. SPIE press, 2001.
- [11] X. Zhu and J. M. Kahn, "Free-space optical communication through atmospheric turbulence channels," *IEEE Trans. Commun.*, vol. 50, no. 8, pp. 1293–1300, 2002.
- [12] T. A. Tsiftsis, H. G. Sandalidis, G. K. Karagiannidis, and M. Uysal, "Optical wireless links with spatial diversity over strong atmospheric turbulence channels," *IEEE Trans. Wireless Commun.*, vol. 8, no. 2, pp. 951–957, 2009.
- [13] M. Karimi and M. Nasiri-Kenari, "BER analysis of cooperative systems in free-space optical networks," *J. Lightw. Technol.*, vol. 27, no. 24, pp. 5639–5647, 2009.
- [14] M. Karimi and M. Nasiri-Kenari, "Free space optical communications via optical amplify-and-forward relaying," *J. Lightw. Technol.*, vol. 29, no. 2, pp. 242–248, 2011.
- [15] L. Zeng, D. O'Brien, H. Minh, G. Faulkner, K. Lee, D. Jung, Y. Oh, and E. T. Won, "High data rate multiple input multiple output (MIMO) optical wireless communications using white LED lighting," *IEEE J. Select. Areas Commun.*, vol. 27, no. 9, pp. 1654–1662, 2009.
- [16] O. Korotkova, N. Farwell, and E. Shchepakina, "Light scintillation in oceanic turbulence," *Waves in Random and Complex Media*, vol. 22, no. 2, pp. 260–266, 2012.
- [17] N. Farwell and O. Korotkova, "Intensity and coherence properties of light in oceanic turbulence," *Optics Communications*, vol. 285, no. 6, pp. 872–875, 2012.
- [18] Y. Ata and Y. Baykal, "Scintillations of optical plane and spherical waves in underwater turbulence," *JOSA A*, vol. 31, no. 7, pp. 1552–1556, 2014.
- [19] H. Gerçekcioğlu, "Bit error rate of focused gaussian beams in weak oceanic turbulence," *JOSA A*, vol. 31, no. 9, pp. 1963–1968, 2014.
- [20] W. C. Cox Jr, *Simulation, modeling, and design of underwater optical communication systems*. North Carolina State University, 2012.
- [21] X. Yi, Z. Li, and Z. Liu, "Underwater optical communication performance for laser beam propagation through weak oceanic turbulence," *Applied Optics*, vol. 54, no. 6, pp. 1273–1278, 2015.
- [22] C. F. Bohren and D. R. Huffman, *Absorption and scattering of light by small particles*. John Wiley & Sons, 2008.
- [23] M. Safari and M. Uysal, "Relay-assisted free-space optical communication," *IEEE Trans. Wireless Commun.*, vol. 7, no. 12, pp. 5441–5449, 2008.
- [24] S. A. Thorpe, *An introduction to ocean turbulence*. Cambridge University Press, 2007.
- [25] E. J. Lee and V. W. Chan, "Part 1: Optical communication over the clear turbulent atmospheric channel using diversity," *IEEE J. Select Areas Commun.*, vol. 22, no. 9, pp. 1896–1906, 2004.
- [26] M. V. Jamali and J. A. Salehi, "On the BER of multiple-input multiple-output underwater wireless optical communication systems," in *4th International Workshop on Optical Wireless Communications (IWOW)*. IEEE, 2015, pp. 26–30.
- [27] G. Einarsson, *Principles of Lightwave Communications*. New York: Wiley, 1996.
- [28] M. Abramowitz and I. A. Stegun, *Handbook of mathematical functions: with formulas, graphs, and mathematical tables*. Courier Corporation, 1970.
- [29] L. Fenton, "The sum of log-normal probability distributions in scatter transmission systems," *Communications Systems, IRE Transactions on*, vol. 8, no. 1, pp. 57–67, 1960.
- [30] M. Jazayerifar and J. A. Salehi, "Atmospheric optical CDMA communication systems via optical orthogonal codes," *IEEE Trans. Commun.*, vol. 54, no. 9, pp. 1614–1623, 2006.
- [31] J. W. Giles and I. N. Bankman, "Underwater optical communications systems. part 2: basic design considerations," in *Military Communications Conference, 2005. MILCOM 2005. IEEE*. IEEE, 2005, pp. 1700–1705.
- [32] C. Abou-Rjeily and A. Slim, "Cooperative diversity for free-space optical communications: transceiver design and performance analysis," *IEEE Trans. Commun.*, vol. 59, no. 3, pp. 658–663, 2011.